2001-8079 C

Proceedings of IMECE'00
2000 ASME International Mechanical Engineering Congress and Exposition
November 5-10, 2000, Orlando, Florida, USA

A PIV METHODOLOGY FOR HIGH-RESOLUTION MEASUREMENT OF FLOW STATISTICS

Eric B. Cummings*
Robert W. Schefer
Sandia National Laboratories
Livermore, California 94551-0969

Jacob N. Chung
Department of Mechanical Engineering
University of Florida
Gainesville, Florida 32611-6300

ABSTRACT

Particle-image velocimetry (PIV) is a flow-diagnostic technique that provides velocity fields from a comparison of images of particulate-laden flow. We have developed a PIV processing methodology that extracts measurements of the particle-displacement histogram from a flow video or ensemble of flow-image pairs. Single-pixel measurement of mean velocity can be obtained from an ensemble of $O(10^3)$ images. Measurements of higher-order moments of the velocity histogram require spatial averaging (i.e., lower spatial resolution), larger ensembles of images, or a combination of the two. We present single-pixel-resolution PIV measurements of a steady microflow and high-resolution measurements of the velocity histogram of a stationary turbulent flow. This methodology has applications in quantifying velocity statistics in other stochastic flows, e.g., bulk and near-wall boiling.

NOMENCLATURE

A amplitude parameter
α, β semi-major and semi-minor axes of the elliptical Gaussian velocity histogram
D effective particle diffusivity
Δt time delay between subimages in correlation pair
$\delta x, \delta y$ Cartesian independent variables of the filter basis function
$\delta x', \delta y'$ independent variables of the filter basis function rotated into the frame of the eccentricity vector
$\mathbf{e}$ eccentricity vector of the elliptical Gaussian velocity histogram
e_x, e_y Cartesian components of the eccentricity vector
$P\{\delta x, \delta y\}$ histogram of particle displacement (nonlinear filter basis function)
σ mean half-width of the velocity histogram
u, v Cartesian components of the electrokinetic velocity vector
u_0, v_0 Cartesian components of the mean velocity vector

INTRODUCTION

Particle-image velocimetry (PIV) is a standard technique for quantifying flow-velocity fields. In PIV, the velocity field is measured by comparing the locations of particles or groups of particles in images of a particulate-laden flow. Often this comparison is performed using image-correlation techniques. In this article we report on extensions of the correlation-based PIV technique to obtain high measurement spatial resolution and the ability to measure velocity statistics accurately and efficiently. These extensions employ ensemble averaging of correlations over a large number flow images. Correlation averaging in PIV is a relatively new procedure (Meinhart et al. (1999); Cummings (2000)) which allows the experimentalist to trade between spatial resolution, temporal resolution, and signal-to-noise ratio (SNR) or measurement accuracy. This flexibility is particularly useful in microsystems, where the spatial resolution of flow images is limited by diffraction. We present single-pixel-resolution measurements of steady electrokinetic flow velocities in microchannels.

Correlation averaging can also be used to measure flow

*Address all correspondence to this author.

DISCLAIMER

statistics in stationary[1], but unsteady, flows. We present single-pixel resolution measurements of velocity histograms at the mid-plane of a circular jet with co-flowing air at Reynolds number 6,100. The procedure of single-pixel correlation is particularly simple and minimizes issues of gradients within the subimage that can distort measuremements. The disadvantage of single-pixel correlation is that a large number of flow images must be processed to obtain useful SNRs. For example, in a steady flow, 1024 image pairs must be processed to obtain a single-pixel correlation similar to a 32×32-pixel subimage correlation of a single frame pair. A factor of 10–1000 more image pairs are required for measuring flow statistics in an unsteady flow. Fortunately, with a processing rate on a standard workstation of ~1 frame pair per second for a 1024×1024-pixel image, ensembles of $O(10^4)$ and even $O(10^5)$ images are practical.

PROCESSING PROCEDURE

The methodology used in this study to obtain high-resolution velocity histograms has been published elsewhere (Cummings (2000)). This methodology involves image pre-processing followed by an iterated sequence of cross correlation, correlation processing, nonlinear filtering to extract measurements, and measurement-grid refinement. The pre-processing phase minimizes sources of velocity bias by background subtraction, flat-field correction, etc. The cross correlation and correlation-processing steps are conducted as in standard PIV. However, the image auto-correlations are also calculated and ultimately used to deconvolve imaging defects, blur, and finite-particle-size effects from the correlations. Following the correlation processing, the correlation field can be related to a velocity histogram. By ensemble averaging over many image pairs, an accurate velocity histogram is constructed without the need for large amounts of spatial averaging in the form a large subimages. The method of single-pixel correlation is unconventional and will be discussed in the next section.

Flow measurements are extracted from these histograms via an optimal nonlinear filter. This filter is a nonlinear least-squares fit of the experimentally obtained histograms to a basis function of the filter having a number of adjustable parameters. The best-fit parameters are the measurements extracted from the histograms, e.g., mean velocity, variance, etc. The filter is optimal when the basis function of the filter properly matches the functional form of the histogram and its dependence upon the adjustable parameters. Different basis functions are presented to account for the different physics of the two flows in this study.

[1]A stationary flow, which has constant *mean* properties, is distinct from a steady flow, which has constant *instantaneous* properties.

SINGLE-PIXEL CORRELATION

In PIV, image correlation is usually performed using the Fourier convolution theorem because of the computational speed of the fast Fourier transform. This transform adds an artificial velocity ambiguity, since it incorrectly treats the image data as spatially periodic. Analysts remove this ambiguity by padding one of the subimages of a pair with null pixels to twice its original size in the row- and column-wise directions before convolving with the other subimage. The measurement resolution is limited by the size of the original unpadded subimage, i.e., measurements that are separated by one unpadded subimage size are independent. The size of the correlation field and hence velocity histogram is set by the size of the padded subimage. By using different amounts of padding, the measurement resolution and histogram width can be varied independently. Taking this procedure to a logical limit, it is possible to pad a single-pixel subimage to a desired histogram width and perform a "single-pixel correlation."

The signal-to-noise ratio (SNR) of a single-pixel correlation from a single image pair is significantly less than unity and must be improved by ensemble averaging in order to obtain a useful measurement. Figure 1 shows the effect of averaging on 16×16-pixel velocity histogram measurements obtained from single-pixel subimages of a turbulent flow. The curves show the histogram of $u - u_0$ at $v = v_0$, where u and v are respectively the row- and column-wise velocities and the subscript '0' denotes the mean value. The top family of curves was measured from a low-turbulence region. The 10^3- and 10^4-image-pair averaged histograms are similar, implying the histogram has converged acceptably at 10^3 averages, analogous to using ~ 32×32-pixel subimages in a single-frame-pair correlation. The 10^2- and 10^3-frame-pair averages have significant differences and the 10-frame-pair and single-frame-pair histograms are completely invalid. The family of histogram measurements at the bottom of Fig. 1 was measured from a relatively turbulent region of the same flow. The 10^3- and 10^4-frame-pair averages are significantly different, indicating the need for $> 10^3$ image pairs for performing such measurements in turbulent regions.

The use of a single-pixel subimage eliminates issues of velocity gradients across the subimage and allows the full measurement resolution permitted by the imaging system to be realized. Furthermore the single-pixel correlation procedure degenerates to multiplying each pixel of the second subimage by the value of the single pixel, a computationally and algorithmically efficient procedure.

STEADY ELECTROKINETIC FLOW IN UNIFORM POST ARRAYS

Electrokinesis is the flow produced by the action of an electric field on a fluid or immersed particle having a net mobile charge. Net charges appear within the nanoscopic Debye layer

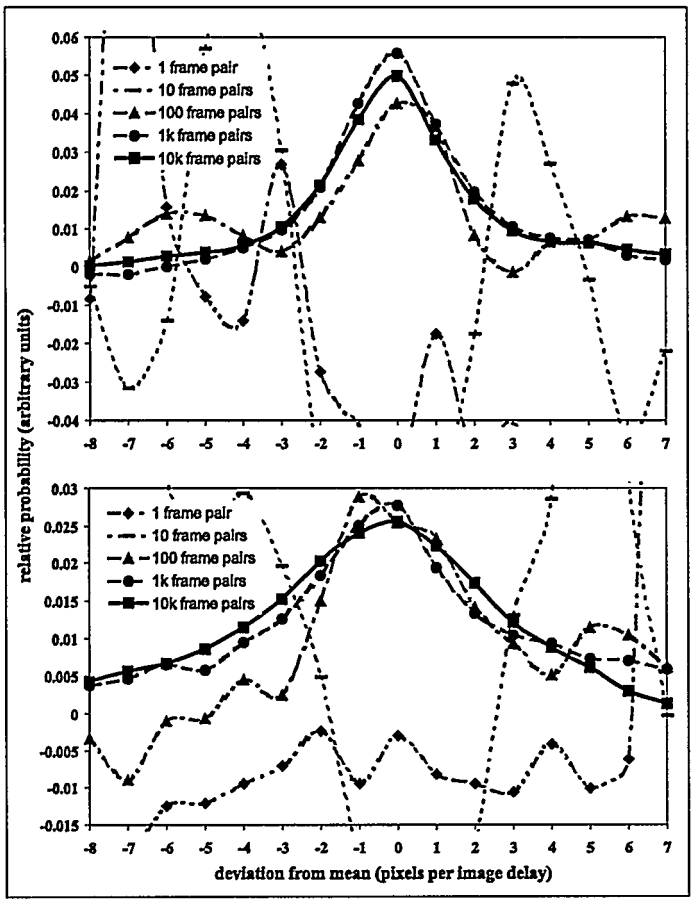

Figure 1. EXPERIMENTALLY MEASURED VELOCITY HISTOGRAMS FROM SINGLE-PIXEL SUBIMAGES IN A TURBULENT FLOW VS. THE NUMBER OF AVERAGED FRAME-PAIR CORRELATIONS. THE CURVES AT THE TOP AND BOTTOM WERE OBTAINED IN LOW AND HIGH-TURBULENCE REGIONS, RESPECTIVELY.

of many liquid/solid interfaces, e.g., water/glass, water/alumina and on many particles in solution, e.g., DNA. This flow achieves significance at the microscale and is of considerable practical importance in microfluidics, since it is a mechanism for manipulating particles and conveying fluids in microsystems using only an applied electric field. The flow rate is linear in the applied field. Furthermore, electrokinetic flow in systems with uniform insulating surfaces and uniform solutions is irrotational with a velocity field everywhere proportional to the electric field. Diffraction-limited, single-pixel-resolution optical diagnostics are often marginal for detailing electrokinesis in real microsystems. The systems chosen for this study are microchannels packed with uniform arrays of posts. Flow in such arrays is amenable to analysis and potentially useful for chemical and particle separations.

BASIS FUNCTION FOR THE NONLINEAR FILTER

The basis function of the nonlinear filter is derived assuming the flow is uniform from the top of the channel to the bottom, as in ideal electroosmosis in a planar system (Cummings et al. (2000)). All marker particles are assumed to have the same electrokinetic mobility and diffusivity. The electrokinetic velocity distribution in the absence of diffusion is a delta function at the mean-flow velocity. When diffusion is present, the velocity distribution spreads into a Gaussian shape. The basis function used in the nonlinear filter is

$$P\{\delta x,\delta y\} = A\exp\left(-\frac{[\delta x - u\Delta t]^2 + [\delta y - v\Delta t]^2}{D\Delta t}\right), \quad (1)$$

where $P\{\delta x,\delta y\}$ is the histogram of particle displacement through $(\delta x,\delta y)$, A is an amplitude scale that can vary across the image. The parameters u and v are the mean electrokinetic velocity components in the row-wise and column-wise directions and D is the effective diffusion coefficient of the particles. The time delay between frames, Δt, can also vary across the image as a result of optimizations. Parameters A and D can only take positive values. This range is ensured by using their logarithms in the external parameter set adjusted by the nonlinear filter. Thus the adjustable parameters of the basis function are u, v, $\log(A)$, and $\log(D)$. The particle diffusivity D is practically constant across the flow. The value of this parameter is initially allowed to be adjusted by the nonlinear filter. The diffusivity field is then fixed at the mean value obtained from the filter in the initial measurement. Thus the filter is given three degrees of freedom: u, v, and $\log(A)$. If the assumptions made in the development of this basis function are rigorously valid and there are no additional complications, such as pressure-driven flow, the filter is optimal. In reality, there are variations in the electrokinetic mobility of the particles that elongate the particle-displacement histogram in the direction of the mean displacement, among other complications. Nevertheless, this basis function usually performs well and has the advantage of simplicity.

EXPERIMENTAL APPARATUS

Figure 2 shows a diagram of the microflow experimental apparatus and micrographs of flow channels filled with post arrays etched in glass. The particle-image recording system in the electrokinetic flow experiments is an inverted 10× video epifluorescence microscope with a blue light-emitting diode ring illuminator. The RS-170 output of the video camera (Cohu 4910) is digitized to 8 bits by a frame grabber (Matrox Meteor) and recorded directly to computer disk. The images are interlaced at 640×480-pixel resolution, with each interlaced field temporally separated by 16.7 ms.

The microfluidic circuit consists of a uniform post array isotropically etched in glass with a thermally bonded glass

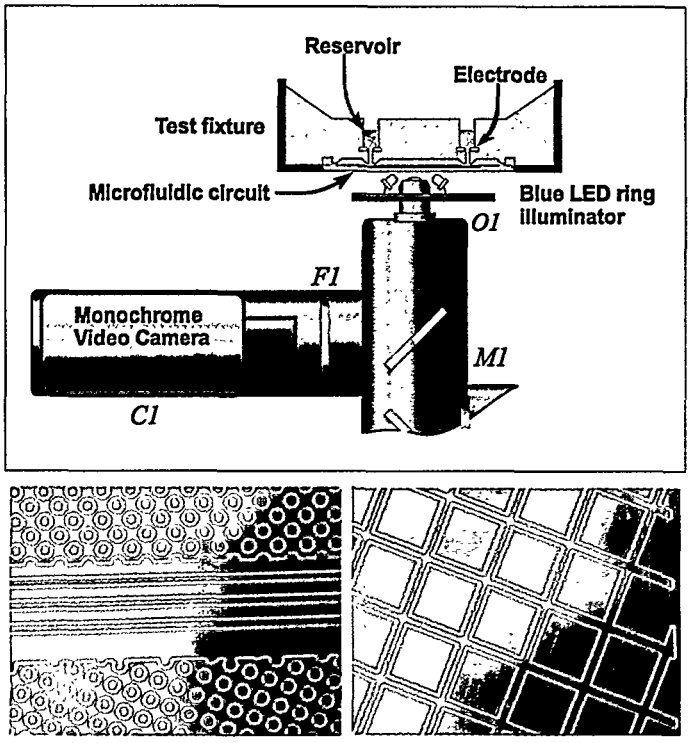

Figure 2. DIAGRAM OF THE EXPERIMENTAL APPARATUS FOR STUDYING ELECTROKINETIC FLOW IN MICROARRAYS AND MICROGRAPHS OF PATTERNED GLASS MICROCHANNELS.

cover slip. Holes drilled in the cover provide access to the microchannels. The circuit is held in place using a 16-port test fixture having gold ring electrodes and 1-ml fluid reservoirs. The channels and reservoirs contain a uniform aqueous suspension of fluorescein-labeled 200-nm latex nanospheres with a carboxalate-modified surface (Molecular Probes, yellow-green fluospheres). The solution is buffered to pH 7.7 by 1-mM phosphate-buffered saline. Voltages are applied to the fixture electrodes via a regulated power supply (HP 6236B or SRS PS350).

The microchannels studied have uniform square arrays of square and circular posts at different angles with respect to the applied electric field. The channels are $\sim 10\,\mu$m deep. The square posts are 142 μm on a side on 200 μm centers. The circular posts are 93 μm in diameter on 200 μm centers.

Care was taken to eliminate pressure-driven flow produced by liquid-level differences in the reservoirs and air currents above the reservoirs. Applied electric fields were kept low enough to avoid particle dielectrophoresis.

RESULTS

Videos of 2,000 sequential interlaced images with 640×480 pixels were processed to obtain independent speed measurements at each image pixel. Figure 3 shows a typical raw particle image from a video. The maximum particle displacement per image delay is ~3 pixels (~150 μm/s). Because the images are sequential, an additional optimization was performed in which up to 32 frames are skipped between correlation pairs so that the particle displacement between correlation pairs is 1–3 pixels (Cummings (2000)). This optimization is performed independently for each velocity measurement, so more frames are skipped in slow-moving regions of the flow than in fast-moving regions, significantly extending the range over which velocities can be measured accurately. Figures 4–7 show measured elec-

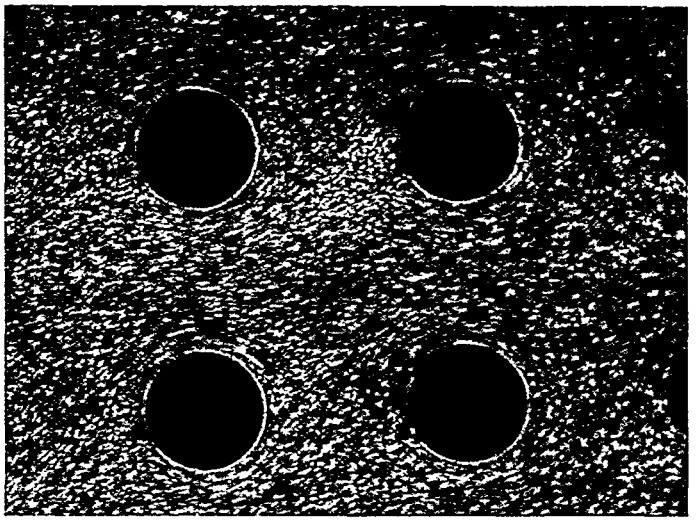

Figure 3. RAW PARTICLE IMAGE USED IN THE ANALYSIS. THE IMAGE SPANS A 520 μM×390 μM RECTANGLE.

trokinetic flow fields. The flow fields are presented in the form of a simulated interferogram. Lines of constant gray scale are contours of constant field. The magnitude of the field at any point can be estimated with reasonable accuracy by counting and interpolating fringes.

Figure 4 shows the measured speed field in a circular post array oriented at 45° with respect to the applied field of 2 V/mm. The flow is from the lower left to the upper right. The fringe spacing is 24.5 μm/s. The speed field throughout the flow can be inferred by counting fringes starting from zero at the stagnation regions in the lower-left and upper-right surfaces of the posts. The streaking patterns that cross the fringes are produced by agglomerated particles having an abnormal surface charge and consequently moving slower or faster than the others. These streaks,

which follow flow streamlines, can be eliminated by thresholding the video images to remove the contributions from particles that are significantly brighter than the average particle. In the measurements shown, the threshold was set to retain some streaking in the image and provide more context for understanding the flow from the figures.

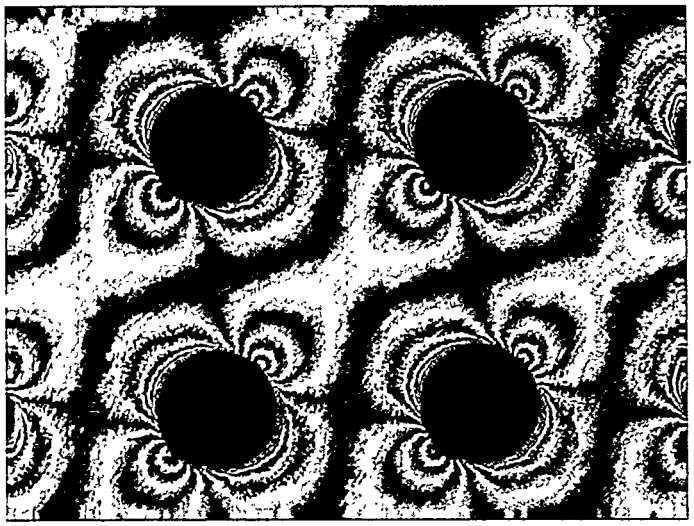

Figure 4. ELECTROKINETIC SPEED FIELD IN AN ARRAY OF CIRCULAR POSTS AT 45° WITH RESPECT TO THE APPLIED ELECTRIC FIELD. THE FRINGE SPACING IS 0.5 PIXELS PER IMAGE DELAY (24.5 μM/S).

Figure 5 shows flow in a similar array of circular posts oriented at 22.5° with respect to the applied field of 2.5 V/mm.

Figure 6 shows u, the row-directed component of the velocity in an array of square posts with channels that are aligned with the electric field of 1 V/mm applied from left to right. The flow slows as it expands into a junction and accelerates as it leaves the junction. The inset expanded image shows the resolution of the flow measurements in the upper right junction. The size of a pixel is indicated by the white square toward the lower right of the inset image.

Figure 7 shows the speed field in an array of square posts at 45° with respect to the applied electric field. The expanded image shown in the inset shows how well the technique works at resolving the speed increase in the region of the sharp post tip. The blemish in the speed field evident in the upper-right channel is real, produced most likely by a localized surface contaminant.

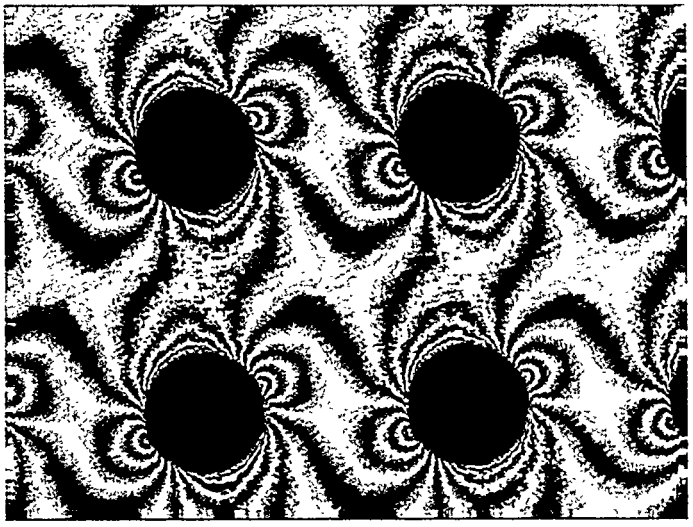

Figure 5. ELECTROKINETIC SPEED FIELD WITHIN AN ARRAY OF CIRCULAR POSTS AT 22.5° WITH RESPECT TO THE APPLIED ELECTRIC FIELD. THE FRINGE SPACING IS 0.5 PIXELS PER IMAGE DELAY (24.5 μM/S).

STATIONARY TURBULENT CIRCULAR JET

Experimental studies of turbulent flows are often conducted for validating numerical submodels and codes. Conventionally, point-measurement techniques like laser-Doppler or hot-wire anemometry are used to obtain turbulent velocity histograms, while imaging techniques like particle-image velocimetry are used to obtain "snapshot" measurements of a flow. While spatial scanning can improve the utility of point measurements, the lack of flow context for the measurements and the typical sparseness of the data can be serious shortcomings. While repetition can improve the utility of snap-shot imaging techniques, spatial resolution is often a shortcoming. Furthermore, it is generally unclear how to present experimental results based on a limited number of snap-shots in a format that is suitable for quantitative model validation.

Image-correlation processing and averaging can be used to obtain velocity correlations and statistics with high spatial resolution. The conventional method of obtaining velocity statistics by particle-image velocimetry is to make independent velocity measurements from a large number of image pairs. This method requires the use of large subimages for correlation to obtain reliable velocity estimates for each image pair. Each image-pair contributes the (estimated) most-probable velocity within the subimage to the histogram. Unfortunately, if a range of velocities is present within the subimage, e.g. if the subimage does not resolve a small-scale turbulent eddy, the information about the velocity distribution other than the most-probable velocity is discarded. Thus the velocity field should be uniform across a subim-

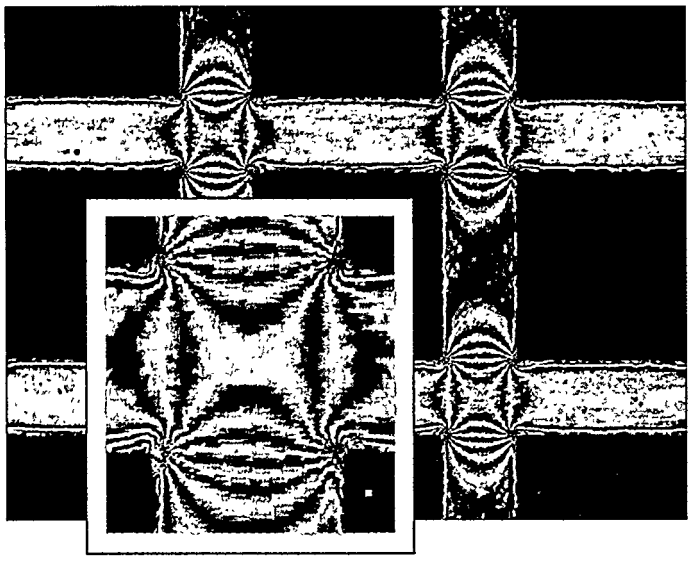

Figure 6. ELECTROKINETIC u VELOCITY FIELD WITHIN AN ARRAY OF SQUARE POSTS AT 0° WITH RESPECT TO THE ELECTRIC FIELD APPLIED FROM LEFT TO RIGHT. THE FRINGE SPACING IS 0.2 PIXELS PER IMAGE DELAY (9.8 μM/S). THE INSET IMAGE SHOWS A DETAIL OF THE FLOW IN THE UPPER-RIGHT JUNCTION. THE WHITE RECTANGLE IN THE INSET SHOWS THE SIZE OF A SINGLE PIXEL.

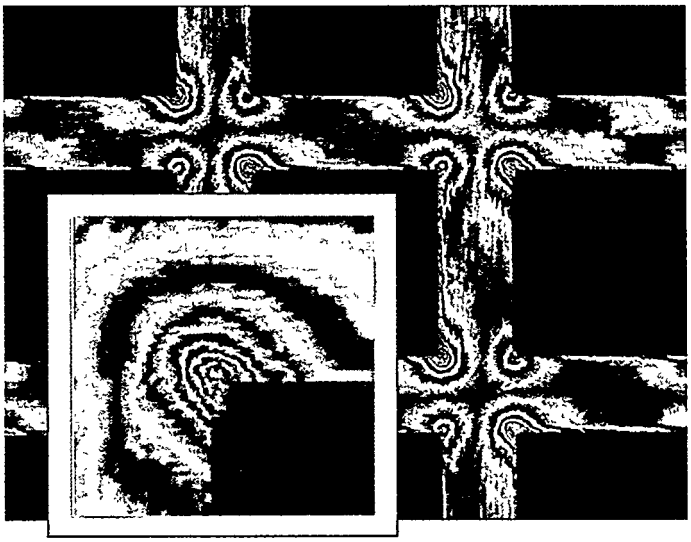

Figure 7. ELECTROKINETIC SPEED FIELD WITHIN AN ARRAY OF SQUARE POSTS AT 45° WITH RESPECT TO THE APPLIED ELECTRIC FIELD. THE FRINGE SPACING IS 0.5 PIXELS PER IMAGE DELAY (24.5 μM/S). THE INSET IMAGE SHOWS A DETAIL OF THE FLOW IN THE UPPER-RIGHT JUNCTION.

age, significantly limiting the range of turbulent length scales that can be properly probed. In contrast, the image-correlation processing and averaging methodology used in this experimental study superimposes estimates from each image pair of the complete velocity distribution within the subimage. The signal-to-noise ratio (SNR) of each individual estimate can be well below unity, since the SNR of the distribution increases as the square root of the number of image pairs in the ensemble. Small, even single-pixel, subimages can be used in the correlation, provided the ensemble is sufficiently large. Furthermore, if multiple-pixel subimages are used, all velocities within the subimage contribute in the correct proportion to the histogram. Thus the velocity-distribution measurement is valid provided only that the flow statistics are uniform across the subimage.

BASIS FUNCTION FOR NONLINEAR FILTER

Unlike the previous basis function, there is no simple general form of a turbulent velocity PDF. However, it was observed that the velocity distributions measured in the jet appeared to have a single peak with an ellipsoidal Gaussian flavor. The eccentricity, orientation, and length of the minor axis of the peak varies throughout the flow. A basis function was chosen to quantify these parameters for comparison with existing data and numerical models. The basis function is

$$P\{\delta x, \delta y\} = A \exp\left(-\left[\frac{\delta x' - u_0 \Delta t}{\alpha \Delta t}\right]^2 - \left[\frac{\delta y' - v_0 \Delta t}{\beta \Delta t}\right]^2 \right), \tag{2}$$

where, u_0 and v_0 are the mean velocity components in the x- and y-directions, respectively, and

$$\alpha \equiv \sigma + ||\mathbf{e}||, \tag{3}$$

$$\beta \equiv \sigma^2/(\sigma + ||\mathbf{e}||). \tag{4}$$

The parameters α and β are the lengths of the semi-major and semi-minor axes of the ellipse. These parameters are derived from σ, the effective half-width of the Gaussian ellipse, and the modulus of the eccentricity vector, $\mathbf{e}$, of the ellipse. The variables $\delta x'$ and $\delta y'$ are derived from δx and δy and $\mathbf{e}$ via

$$\delta x' \equiv \frac{e_x \delta x + e_y \delta y}{||\mathbf{e}||}, \quad \text{and} \tag{5}$$

$$\delta y' \equiv \frac{e_y \delta x - e_x \delta y}{||\mathbf{e}||}, \tag{6}$$

where e_x and e_y are the components of the eccentricity vector in the x- and y-directions, respectively. Again, parameters that

can range from $(0,\infty)$, i.e., A and σ, are mapped to external parameters that can range from $(-\infty,\infty)$ by taking logarithms. This mapping reduces stiffness and other difficulties with the numerical filter. The external parameters of the basis function are $\log(A)$, u_0, v_0, $\log(\sigma)$, e_x, and e_y. The external parameters of the same function may be expressed in a variety of different ways, e.g., in polar rather than Cartesian coordinates. However, the numerical implementation of the optimal nonlinear filter is more robust with this choice of parametrization than others that were attempted.

EXPERIMENTAL APPARATUS

The turbulent flow that was studied consists of an axisymmetric, central air jet surrounded by a low-velocity co-flowing air stream. The central jet tube has a 5.3-mm inside diameter and a 6.8-mm outer diameter. The straight jet tube is 1-m long, which ensures a fully-developed turbulent pipe flow velocity distribution at the jet exit. The outer co-flowing air stream has a 75-mm outer diameter, and passes through a honeycomb section to produce a uniform laminar flow.

The central-jet bulk velocity is 18.2 m/s, giving a Reynolds number based on the jet exit diameter of 6,100. The co-flowing air velocity is 0.96 m/s. Bulk velocity of the fuel jet was determined from the measured volumetric flow rates and the internal area of the jet nozzle. The gas-flow rate of the central jet and the co-flow are metered by mass-flow controllers to an accuracy of 2%.

The PIV system uses the output of a double-pulsed Nd:YAG laser (Spectra Physics PIV-400, 400 mJ/pulse at 532 nm) to illuminate seed particles added to the flow. The beam is formed into a 75-mm high laser sheet approximately 250-μm thick by cylindrical optics and subsequently passed through the test section. Mie-scattered light from the seed particles is collected by a 105-mm focal length, f2.8 camera lens and detected using a CCD video camera with a 1024×1024-pixel array (TSI Model 630045 Cross-correlation Camera). Particle images illuminated by the two laser pulses are recorded on sequential video frames using a frame-straddle technique. The delay time between particle images is 10 μs, which provides a particle displacement of ~10 pixels at the maximum velocity. The field of view of the images is 49×49 mm, providing a resolution of 48 μm/pixel. A 10-nm bandwidth interference filter centered at the laser wavelength of 532 nm placed in front of the collection lens eliminates background room light.

Seed particles in the both the fuel jet and co-flowing air were supplied by a fluidized-bed seeder. The seed particles are nominally-300-nm ceramic Zeeospheres manufactured by the 3M Corporation. Calculations show that this size is sufficiently small for the particles to accurately follow the gas flow at the flow conditions studied. Cyclone separators located downstream of the seeders remove particle agglomerates and improve the particle-size uniformity.

RESULTS

An ensemble of 14,500 image pairs of this turbulent flow was processed to obtain independent velocity histograms at 8×8-pixel and single-pixel resolutions. The mean speed fields measured at the lower and higher spatial resolution are shown in Figs. 8 and 9, respectively. The peak speed is ~ 18.2 m/s or ~ 10 pixels per frame at the base of the jet. The correlation window size in the single-pixel analysis is 8×8 pixels, allowing velocity fluctuations of ±4 pixels per image delay to be recorded.

Figure 10 shows the variance and peak-correlation-amplitude fields across the flow. As expected, the variance is largest at the edge of the base of the jet. The potential core of the jet disappears about two exit-diameters downstream of the nozzle. The peak correlation amplitude decreases by an order of magnitude from the ambient air to the center of the jet because of the combined effect of the higher variance and increased out-of-plane particle motion in the jet.

Figure 11 shows the components e_x and e_y of the eccentricity vector, **e**, where the x- and y-directions are aligned with the rows and columns, respectively. The full scales of the variation of these parameters is less than a pixel in these measurements, i.e., the ellipsoidal correlation peak is elongated by less than a complete pixel. The measurement could be made less noisy by using a longer time delay between images at the cost of spatial resolution or by using a larger ensemble of images at the cost of increased processing and experiment durations.

The eccentricity fields in Fig. 11 contain a systematic error. Figures 8 and 9 show thatthe mean-velocity gradients at the base of the jet are too large for the approximation of uniform properties across an 8×8-pixel subimage made in deriving the filter basis function (2). A velocity gradient across the subimage appears as an artificially increased eccentricity vector in the direction of the mean flow. To remove this artifice, the analyst could either use smaller subimages at the expense of SNR, revise the filter basis function to accommodate velocity gradients, or post-process the eccentricity field using the measured velocity field. The post-processing procedure is possible because of the simple form of the velocity-gradient effect on eccentricity vector and variance measurements.

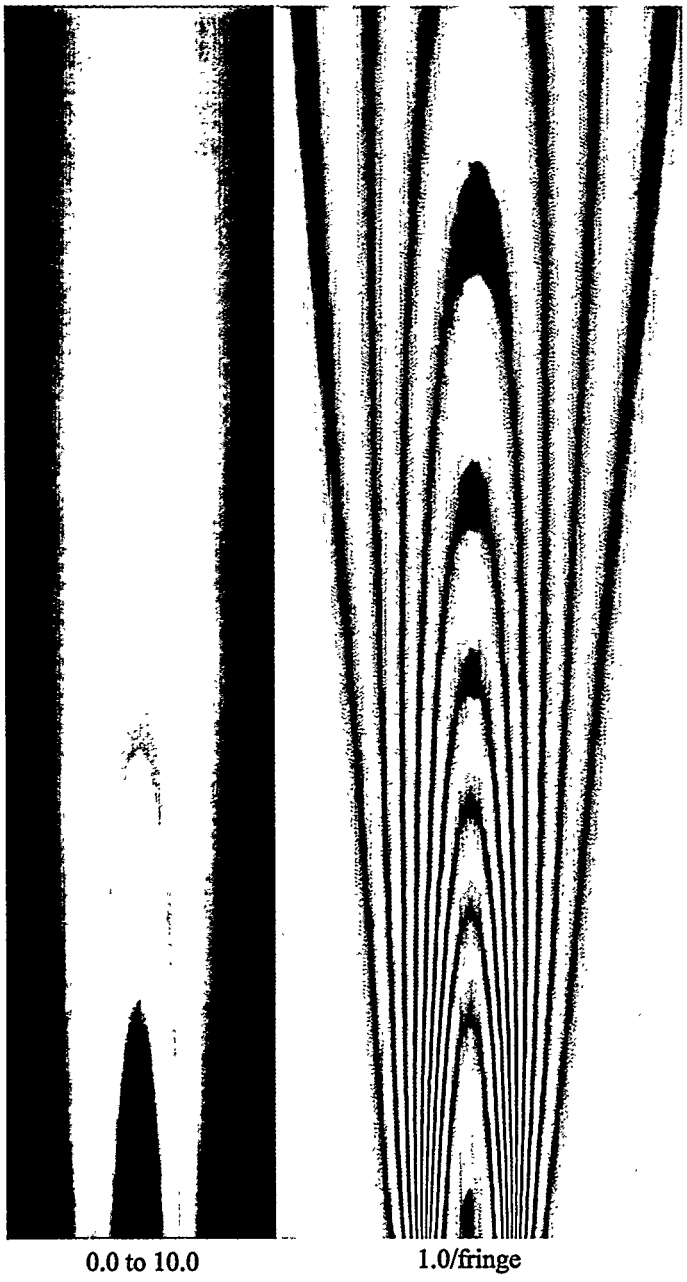

Figure 8. COLOR MAP AND SIMULATED INTERFEROGRAM OF THE SPEED FIELD IN THE TURBULENT JET MEASURED WITH 8×8-PIXEL SUBIMAGES. RED CORRESPONDS TO ZERO SPEED AND BLUE CORRESPONDS TO 10 PIXELS DISPLACEMENT BETWEEN IMAGES.

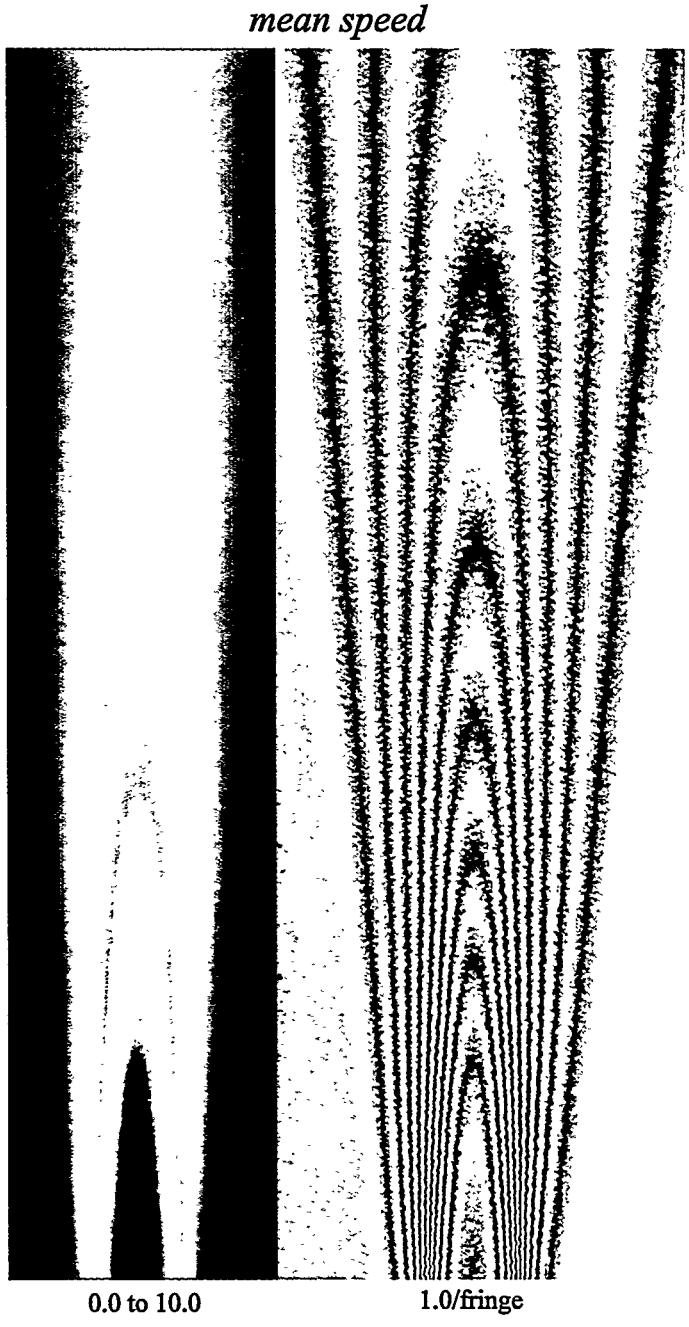

Figure 9. COLOR MAP AND SIMULATED INTERFEROGRAM OF THE SPEED FIELD IN THE TURBULENT JET MEASURED WITH SINGLE-PIXEL SUBIMAGES. RED CORRESPONDS TO ZERO SPEED AND BLUE CORRESPONDS TO 10 PIXELS DISPLACEMENT BETWEEN IMAGES.

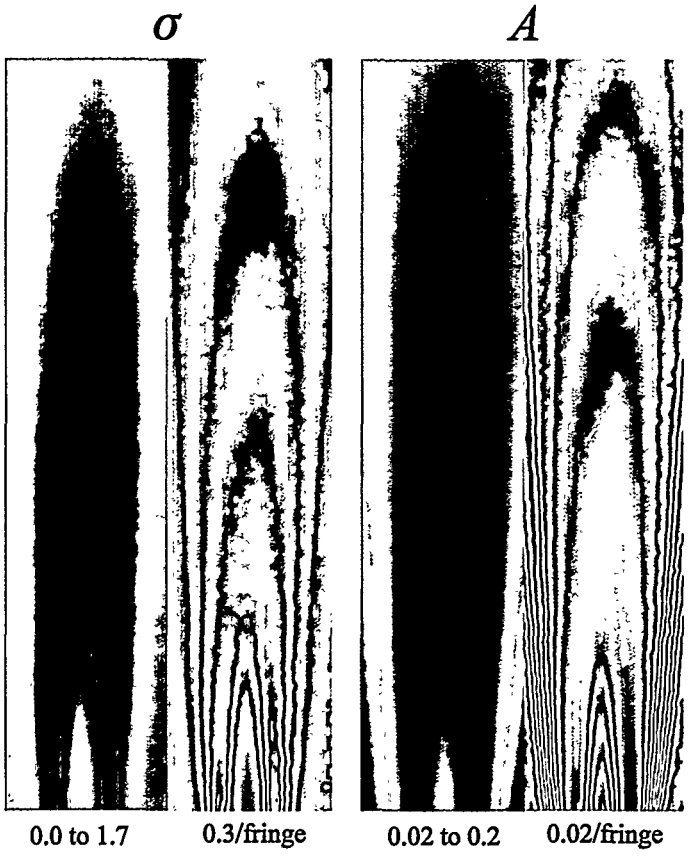

Figure 10. COLOR MAP AND SIMULATED INTERFEROGRAM OF THE COMPONENTS OF THE EFFECTIVE VARIANCE (σ) AND PEAK CORRELATION AMPLITUDE (A) MEASURED WITH 8×8-PIXEL SUBIMAGES. THE COLOR-MAP RANGES AND FRINGE SPACINGS ARE INDICATED BENEATH THE IMAGE. THE UNITS OF THE VARIANCE ARE PIXELS/IMAGE DELAY AND THE UNITS OF THE AMPLITUDE ARE ARBITRARY.

Figure 11. COLOR MAP AND SIMULATED INTERFEROGRAM OF THE COMPONENTS OF THE ECCENTRICITY VECTOR MEASURED WITH 8×8-PIXEL SUBIMAGES. THE COLOR-MAP RANGES AND FRINGE SPACINGS ARE INDICATED BENEATH THE IMAGE IN UNITS OF PIXELS/IMAGE DELAY.

CONCLUSIONS

Particle image velocimetry can be applied to obtain high-spatial-resolution and high-accuracy velocity statistics of stationary but not necessarily steady flows. Accurate single-pixel-resolution velocity measurements of a steady flow can be made by ensemble averaging the correlations of $O(10^3)$ image pairs. Accurate measurements of velocity histograms can be made of a turbulent flow given a data set with $O(10^4$–$10^5)$ images, with the lower and upper range sufficient for 8×8-pixel and single-pixel subimages, respectively. The storage and processing requirements for this size of data set are no longer prohibitive or particularly challenging. A more-serious problem is the need to maintain a stationary flow for $O(10)$ hours to record the image set using standard high-resolution PIV cameras which can typically record only $O(1)$ image-pair per second. Given the ability to make single-pixel measurements, experimentalists may reconsider the need for megapixel and multi-megapixel cameras with relatively low data throughput.

The statistical measurement capabilities of PIV could be used to study other flow phenomena having a strong stochastic component, such as boiling and natural and forced convection. The potential for sub-micrometer resolution of velocity histograms makes it possible to study these phenomena at the microscale, providing a new window into fundamental heat-transfer. The need for particle seeding can be troublesome for some boiling studies, since particles serve as bubble nucleation sites and can thus perturb the flow behavior. However, the seeding density, size distribution, and hydrophilicity of the particle markers can be tailored to mimic those of particles that are intrinsic to a practical boiling system. Commercially available flu-

orescent latex microspheres that we have tested are not stable at the atmospheric boiling point of water, thus either Mie-scattering particles or improved fluorescent markers may need to be employed.

ACKNOWLEDGMENT

This work was funded by a Sandia Engineering Sciences LDRD. Sandia is a multi-program laboratory operated by Sandia Corporation, a Lockheed-Martin company, for the United States Department of Energy under contract DE-AC04094AL85000.

REFERENCES

Cummings, E. B. (2000) "An image processing and optimal nonlinear filtering technique for particle image velocimetry of microflows," to be published in *Exper. in Fluids.*

Cummings, E. B., Griffiths, S. K., Nilson, R. H., Paul, P. H. (2000) "Conditions for similitude between the fluid velocity and electric field in electroosmosis," *Anal. Chem.*, **72**, pp 2526–2532.

Meinhart, C. D., Wereley, S. T, Santiago, J. G. (1999) "A PIV Algorithm for Estimating Time-Averaged Velocity Fields," ASME/JSME Fluids Engineering Conference, San Francisco, CA, July 18–23, FEDSM 99-7261.